

# Observable Statistical Mechanics

Lodovico Scarpa,<sup>1,\*</sup> Abdulla Alhajri,<sup>1,2</sup> Vlatko Vedral,<sup>1</sup> and Fabio Anza<sup>3,†</sup>

<sup>1</sup>*Clarendon Laboratory, University of Oxford, Parks Road, Oxford OX1 3PU, UK*

<sup>2</sup>*Quantum Research Centre, Technology Innovation Institute, 9639 Abu Dhabi, United Arab Emirates*

<sup>3</sup>*Department of Mathematics, Informatics and Geosciences, University of Trieste, Trieste, Italy*

(Dated: July 27, 2024)

Understanding equilibration and thermalization in isolated many-body quantum systems is a central challenge in quantum physics. The traditional approach focuses on the study of the full state of the quantum system which, at equilibrium, is best described by the Diagonal Ensemble. Here, we present Observable Statistical Mechanics, a novel paradigm that shifts attention from the full quantum state to the statistics of measurement outcomes. This approach is grounded in the Maximum Observable Entropy Principle, positing that equilibrium measurement statistics tend to maximize observable entropy under conserved average energy. By focusing on accessible measurements, the theory accurately predicts equilibrium probability distributions without needing detailed microscopic information like the energy eigenstates. Extensive numerical experiments on 7 spin-1/2 Hamiltonians demonstrate the broad applicability and robustness of this framework.

The dynamics of interacting, many-body quantum systems present a rich tapestry of phenomena that challenge our understanding of equilibration and thermalization. At the core of this field lie various fundamental questions: How do isolated quantum systems reach equilibrium? What determines their long-term behavior, and how can we predict it?

The mechanism of dynamical equilibration [1–13] in isolated quantum systems is primarily driven by dephasing—the loss of coherence between different energy eigenstates. This process leads to stationary behavior for observable quantities, even as the underlying quantum state evolves unitarily.

With respect to their equilibrium phenomenology, traditionally, quantum systems have been classified into two broad categories: quantum chaotic [14–17] and quantum integrable [18–22]. While chaotic systems are expected to exhibit thermal behavior via the Eigenstate Thermalization Hypothesis [14, 23–31], integrable systems often equilibrate to more complex states described by the Generalized Gibbs Ensemble (GGE) [18, 19]. This dichotomy, however, only scratches the surface of the intricate dynamics at play.

Complementing the ETH, both the concept of dynamical typicality [3, 32–40] and studies in Random Matrix Theory [16, 41–46], suggest that most initial states and local Hamiltonians of a large quantum system will lead to similar dynamical behavior. This offers a powerful statistical approach to equilibration and thermalization.

On the other hand, in the past twenty years, we have discovered several ways to hinder thermalization and even equilibration. Many-body localization (MBL) [47–49] has proven that some disordered quantum systems can evade local thermalization entirely. Other noteworthy phenomena include pre-thermalization [50–52], quantum scars [53, 54], Hilbert space fragmentation [54, 55]

and dynamical symmetries [56–58]. These discoveries challenge our understanding of equilibration and thermalization, thus inviting further investigations and new approaches. Notable examples are the most recent studies in Random Unitary Circuits [59, 60] and the emergence of Measurement-Induced Entanglement Phase Transitions [61–63].

Within this complex landscape, an entirely new perspective has recently emerged: the focus on observable entropy [64–70]. This approach shifts the attention from the full state to the statistics of measurement outcomes, offering a new perspective on equilibration and thermalization. By focusing on accessible measurements, one can capture essential features of the system’s behavior without requiring complete knowledge of its microscopic details [64, 65, 67, 68].

Advancing this new perspective, in this work, we lay out a novel framework—Observable Statistical Mechanics—that leverages the concept of observable entropy to accurately predict equilibrium properties of observables in quantum many-body systems. Our analytical development is paired with large-scale numerical experiments that provide empirical support to the theory. This demonstrates the broad applicability and robustness of Observable Statistical Mechanics.

## I. RESULTS

### A. Setup

We consider a many-body quantum system made by  $N$  interacting units, each of dimension  $d$ , and thus with Hilbert space  $\mathcal{H}$  of dimension  $D = d^N$ . The entire system evolves with Hamiltonian  $H = \sum_n E_n |E_n\rangle\langle E_n|$ , and it is initialized in a pure state  $|\psi_0\rangle = \sum_n c_n |E_n\rangle \in \mathcal{H}$ . We consider an observable  $A := \sum_{j=1}^{n_A} a_j A_j$  where the eigenprojectors are defined as  $A_j := \sum_{s=1}^{d_j} |j, s\rangle\langle j, s|$ , with  $n_A$  the number of distinct eigenvalues. This identifies a de-

\* lodovico.scarpa@physics.ox.ac.uk

† fabio.anza@units.it

composition of the full Hilbert space into  $n_A$  subspaces  $\{\mathcal{H}_j\}_{j=1}^{n_A}$ , each of dimension  $d_j := \dim \mathcal{H}_j = \text{Tr } A_j$ , in which the measurements have definite outcomes:  $\mathcal{H} = \bigoplus_{j=1}^{n_A} \mathcal{H}_j$ . Note that throughout the paper we refer to “observables”, but all results can be equivalently phrased in terms of a series of compatible measurements, which together define a projection-valued measurement (PVM) scheme  $\mathcal{A} = \{A_j\}_{j=1}^{n_A}$ :  $A_j A_k = \delta_{jk} A_j$ ,  $\sum_{j=1}^{n_A} A_j = \mathbb{I}$  with a total number of  $n_A$  classically distinguishable outcomes. The framework can also be generalized to positive operator-valued measurements (POVMs). Moreover, we focus on highly degenerate observables. Indeed, in realistic experiments, the number of classically distinguishable outcomes is limited compared to the full dimension of the Hilbert space  $n_A \ll D$ . Since  $\sum_{j=1}^{n_A} d_j = D$ , this means we are always in the situation in which  $\log d_j \gg 1$  and, in most cases  $\log d_j \sim N$ . Typical examples are von Neumann macro-observables and observables with support on less than half of the entire system [65].

The time-dependent probability distribution of the measurement outcomes  $p_j(t) := \langle \psi_t | A_j | \psi_t \rangle$  evolves as a result of the global unitary dynamics as

$$p_j(t) := \sum_{n,m} c_n^* c_m e^{\frac{i}{\hbar}(E_n - E_m)t} [A_j]_{nm}, \quad (1)$$

with  $[A_j]_{nm} := \langle E_n | A_j | E_m \rangle$ . In general, when the system is many-body and interacting the energy spectrum is non-degenerate and has non-degenerate energy gaps [1–3, 5–7, 27, 39, 71–73]. These conditions lead to a central result in the study of equilibrium in closed quantum systems [10, 11]: *If a system equilibrates, it will do so to the predictions of the diagonal ensemble*  $\rho_{DE} := \sum_n |c_n|^2 |E_n\rangle\langle E_n|$ . Defining  $p_j^{DE} := \text{Tr}(\rho_{DE} A_j) = \sum_n |c_n|^2 [A_j]_{nn}$ , we indicate this phenomenology with the following notation

$$p_j(t) \rightsquigarrow p_j^{DE}. \quad (2)$$

Moreover, it is important to mention that both the non-degenerate energy spectrum and non-degenerate energy gaps assumptions can actually be relaxed [5, 6, 43, 71, 74–77]. Direct computation of  $\rho_{DE}$  is often unfeasible as it requires knowledge of an exponentially large number of energy eigenstates. The issue of understanding and predicting equilibrium then becomes: *How can we access  $p_j^{DE}$  without the energy eigenstates?* This work presents a novel, principled solution to this problem, with abundant analytical and numerical evidence supporting it—the *Maximum Observable Entropy Principle* (MOEP). Beyond the notation that has already been introduced, the main actors are the entropy of the energy distribution  $S(H) = -\sum_n |c_n|^2 \log |c_n|^2$ , the equilibrium entropy of a generic basis diagonalizing all our measurements  $\tilde{S}(A) := -\sum_{j=1}^{n_A} \sum_{s=1}^{d_j} p_{js}^{DE} \log p_{js}^{DE}$ , with  $p_{js}^{DE} := \langle j, s | \rho_{DE} | j, s \rangle = \sum_n |c_n|^2 |\langle E_n | j, s \rangle|^2$ , and the equilibrium entropy of the observable  $S(A) := -\sum_{j=1}^{n_A} p_j^{DE} \log p_j^{DE}$ , where the two are related via  $p_j^{DE} = \sum_{s=1}^{d_j} p_{js}^{DE}$ .

## B. Maximum Observable Entropy Principle

Estimating  $p_j^{DE}$  to a good degree of accuracy while lacking complete information (the energy eigenstates) can be phrased as a standard inference problem. While virtually all efforts in the literature have been focused on building the entire  $\rho_{DE}$  (e.g. the GGE construction [18, 19]), this approach is often too demanding and can easily fail: it is sufficient that one observable does not agree with the prediction. It also does not consider that we only have access to a limited number of observables in most experiments. Instead, inferring directly the probability distribution of our measurement outcomes is a minimal and more practical route. This leads to the following principle.

**Definition I.1** (Maximum Observable Entropy Principle). *At equilibrium, the observed measurement statistics  $p_j^{DE}$  is described by the distribution that maximizes its entropy, under perturbations with conserved average energy.*

While first formulated to study the emergence of thermal equilibrium [64–66], its predictive capabilities appear to go well beyond its initial intent, as we will show explicitly in the following. We begin by discussing a simple heuristic argument that points towards the validity of MOEP in highly degenerate observables. This will help the reader gain intuition on this principle. We then present analytical predictions of MOEP and showcase their validity in a large-scale numerical experiment.

## C. Heuristics

The posited Maximum Observable Entropy Principle states that our best guess for  $p_j^{DE} = \sum_s p_{js}^{DE}$  is the distribution resulting from the constrained maximization of  $\tilde{S}(A)$ . In principle, all (linearly independent) conserved quantities should be included as constraints — normalization and the expectations of all energy eigenstates  $|c_n|^2$ . Including all of them invariably leads to the correct result  $p_j^{DE}$ , but it requires knowledge of all energy eigenstates [78]. The core intuition behind MOEP is that including all  $|c_n|^2$  is not needed in most cases. Due to the expected shape of  $|c_n|^2$ , peaked on a micro-canonical window but random inside it, knowledge of the average  $E = \sum_n |c_n|^2 E_n$  should be sufficient to extract an accurate estimate. At the information-theoretic level, this is because physically accessible observables will be highly degenerate,  $\log d_j \sim N$ , and therefore can not retain too many details about the conserved quantities. Indeed, the equilibrium mutual information  $I_{eq}(H, A)$  between the energy and our measurement can be shown to be negligible  $I_{eq}(H, A) \approx 0$ , and vanishing in the thermodynamic limit  $N \rightarrow \infty$ . All details are given in the Methods section.

Beyond the information-theoretic aspect, here we provide another heuristic for the validity of MOEP, leverag-

ing the entropic uncertainty principle [79, 80]. Given a basis that diagonalizes our observable  $\{|j, s\rangle\}_{j=1, s=1}^{n_A, d_j}$  and the energy eigenbasis  $\{|E_n\rangle\}$  we have  $\tilde{S}(A) + S(H) \geq -\log c(A, H)$ , where  $c(A, H) := \max_{j, s, n} |\langle E_n | j, s \rangle|^2$  and  $S(H) = -\sum_n |c_n|^2 \log |c_n|^2$  is the entropy of the energy distribution. The quantity  $c(A, H)$  can be estimated using the main result in [65], leading to  $-\log c(A, H) \geq \frac{1}{2} \log D$ . Moreover, since Reimann's work [1] it has been accepted that realistic and thermodynamically stable initial states of a mesoscopic system have an energy distribution that is localized within a microcanonical window. This means the entropy  $S(H)$  is much smaller than its maximum value:  $S(H) \ll \log D \sim N$ . This leads to the expectation that our observable has an eigenbasis  $\{|j, s\rangle\}$  with entropy that is expected to scale linearly with system size:  $\tilde{S}_A \sim N$ . This is a hallmark of the emergence of statistical mechanics for measurement outcomes rather than states. This can be established following Jaynes' work [81–83], using a maximum entropy principle. This heuristic argument is made more rigorous in the Methods section by arguing a realistic lower bound to  $\tilde{S}_A$ .

#### D. Observable Statistical Mechanics

Throughout the paper, we provide numerical evidence supporting the analytical statements and the ensuing predictions of the theory. The full details of the numerics are given in the methods section, but here we give a quick summary: the parameters of the models, initial states and observables chosen. We focused on 1D spin-1/2 models with nearest neighbor interactions and magnetic field. Our Hamiltonians are all translational invariant so that the parameters of the model are the nearest neighbor interaction constants  $\vec{J}$  and the magnetic field  $\vec{B}$ . We investigated 7 different Hamiltonian models, spanning through quantum integrable and quantum chaotic and with system sizes up to  $N = 20$ . The explicit values are given in table I. We looked at 5 different initial states  $|\psi_0(\theta_m)\rangle$ , with  $m \in \{1, 5, 10, 15, 20\}$ . These are all tensor product states with Neel order, but aligned along different axes. For  $m = 1$  the initial state is aligned along  $z$  while for  $m = 20$  it is aligned along  $x$ . The rest are aligned along an axis forming an angle  $\theta = \frac{m-1}{19} \frac{\pi}{2}$  with the  $z$  axis, in the  $z - x$  plane. For all Hamiltonian models and all initial states, we studied 6 classes of observables, three one-body and three two-body:  $\sigma_i^x, \sigma_i^y, \sigma_i^z, \sigma_i^x \sigma_{i+1}^x, \sigma_i^y \sigma_{i+1}^y, \sigma_i^z \sigma_{i+1}^z$ , with  $i = 1, \dots, N$ .

We now present the complete theory of Observable Statistical Mechanics, with its main predictions and analytical results.

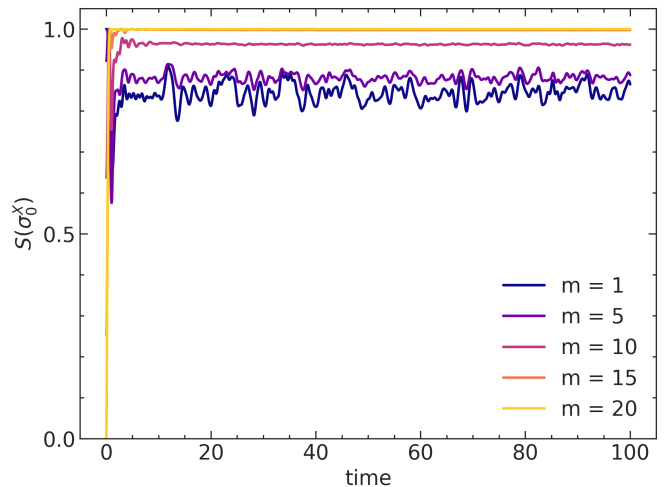


Figure 1: Time evolution of the Shannon entropy  $S(A)$  for model  $J = (0, 0, 1)$  &  $B = (0.9045, 0, 0.8090)$ , observable  $\sigma_0^x$  and all the initial states considered (labeled by  $m$ ), for  $N = 20$ . Note the constrained maximum can be lower than the absolute maximum. In fact, this plot has been chosen to highlight the above point, and in other models, for the same observable, entropy equilibrates around the absolute maximum for every initial state. See appendix A.

##### 1. Dynamical Relaxation to Max Observable Entropy

Since Observable Statistical Mechanics is based on the Maximum Observable Entropy Principle, we checked that the Observable Entropy exhibits relaxation towards a high-entropy stationary state. We indeed observe this behavior for almost models, initial states and observables considered. An example is given in fig.1, while additional plots are included in appendix A. This shows numerical evidence of a dynamical tendency to evolve and settle on high observable entropy configurations—a necessary prerequisite for the validity of the theory. It also supports the heuristic arguments presented before that the stationary value of the entropy, computed from the Diagonal Ensemble distribution  $p_j^{DE}$ , can be characterized via the Maximum Observable Entropy Principle. These findings agree and are well supported by independent studies [70].

##### 2. Equilibrium Equations

We proceed by introducing the equilibrium equations of Observable Statistical Mechanics, together with their general solution and an ensuing novel prediction.

The constrained maximization of  $\tilde{S}_A$  can be solved using the Lagrange multipliers techniques [64, 84]. As discussed above, we keep only the normalization of probabilities and average energy constraints. After various algebraic manipulations, which are detailed in the Methods section III B, we find that when a highly-degenerate observable  $A$  satisfies the MOEP its distribution  $p_j^{DE}$  will

obey the following Equilibrium Equation:

$$-p_j^{DE} \log p_j^{DE} + p_j^{DE} \log d_j \stackrel{\text{eq}}{=} \lambda_A p_j^{DE} + \beta_A R_j^{DE}, \quad (3)$$

where

$$R_j^{DE} := \text{Tr}(A_j H \rho_{DE}) = \sum_n |c_n|^2 E_n [A_j]_{nn}, \quad (4)$$

and  $\lambda_A, \beta_A$  are the Lagrange multipliers associated with the normalization and average energy constraint, respectively. Despite eq.(3) being highly non-linear and exhibiting an implicit dependence on  $p_j^{DE}$ , there is one and only one form of the equilibrium probability distribution that is compatible with a maximum entropy characterization: the exponential distribution. This follows straightforwardly from Gibbs' inequality [83, 85]. Properly parameterized for future convenience, this leads to

$$p_j^{DE} = \frac{d_j e^{-\beta_A \varepsilon_j}}{\mathcal{Z}_A} \quad \mathcal{Z}_A = \sum_j d_j e^{-\beta_A \varepsilon_j} \quad (5)$$

where  $\varepsilon_j$  is an observable-specific quantity with the dimension of energy such that  $\sum_j p_j^{DE} \varepsilon_j = E$ , and  $\mathcal{Z}_A$  is a measurement-specific partition function. Its meaning is understood and it will be discussed in subsection ID 5.

### 3. A special solution: Hamiltonian Unbiased Observables

While the most general solution of the Equilibrium Equations, eq.(5), is given here for the first time, a special case has been previously studied in [64, 65]:  $p_j = \frac{d_j}{D}$ . This is the equilibrium distribution of a large class of observables, named ‘‘Hamiltonian Unbiased Observables’’ (HUOs), for which  $\varepsilon_j = E \forall j$ . These are observables which are diagonal in a basis that is unbiased [79, 86–88] with respect to the energy basis:  $\langle E_n | j, s \rangle = \frac{e^{i\theta_{js}^n}}{\sqrt{D}}$ . Such basis is accordingly called ‘‘Hamiltonian Unbiased Basis’’ (HUB). Physically, these observables do not possess any information about the energy; in fact, in III A 2 we show their mutual information with the Hamiltonian is zero. HUOs are a very useful model to understand thermalization, for three reasons. First, it has been proven analytically that the ETH holds for all of them [64], so they will generically thermalize under standard assumptions. Second, in a statistically precise sense (Haar measure), most observables are expected to be quite close to being HUOs. This was proven in ref.[65], along with other statements clarifying their physical relevance, namely their relation to highly degenerate observables. Third, using them we can determine extensive sets of thermal observables in MBL systems. Indeed, while it is true that MBL systems escape quantum statistical mechanics in the standard sense, there are several local observables that still exhibit MOEP, even in the localized phase [66, 89].

While HUOs capture core aspects of observable thermalization, they have one major drawback: they are insensitive to the overall energy scale of the system. This is because their equilibrium mutual information with the energy vanishes identically. We do not expect this to hold exactly for physical observables which, at equilibrium, do exhibit a smooth dependence on the energy scale of the system. Nevertheless, we believe the core mechanism to be approximately correct. In other words, we expect a non-vanishing but very small equilibrium mutual information between the observable and energy distributions.

### 4. A novel prediction

Solutions of eq.(3) must be of the form given in eq.(5), but their existence is not guaranteed: they must satisfy eq.(3). Plugging the general solution into the Equilibrium Equation, we obtain

$$R_j^{DE} = \varepsilon_j p_j^{DE}. \quad (6)$$

Together, eqs.(3),(5) and (6) constitute our first result: we have an exact solution to the equilibrium equation, which leads to a novel and highly non-trivial prediction. Its validity guarantees that  $p_j^{DE}$  indeed satisfies the equilibrium equation.

That the quantity  $\varepsilon_j$  must exist and that  $\varepsilon_j \in [E - \Delta E/2, E + \Delta E/2]$  can be shown analytically. The details are given in section III C. Moreover, the validity of eq.(6) is numerically verified to a high degree of accuracy. To see the dynamically-emergent linearity, we use a time-implicit plot ( $p_j(t), R_j(t)$ ). For each such plot, we compute the (absolute value of the) Pearson correlation coefficient, which quantifies the linear correlation between the two sets  $\{p_j(t)\}$  and  $\{R_j(t)\}$ , with a value of 1 corresponding to perfect linearity [90]. In figure 2, we give the histogram of the Pearson coefficients, which clearly shows that the vast majority of values is close to 1. Moreover, the inset shows an example of the 2D histogram of a plot of  $R_j(t)$  against  $p_j(t)$ , where the linear behaviour is also evident. Thus, we have strong numerical support for eq.(6).

### 5. An observable-specific notion of energy.

To obtain a complete solution, we need to fix the value of the Lagrange multiplier  $\beta_A$  by using the energy constraint:

$$\beta_A : \sum_j p_j^{DE} \varepsilon_j = -\frac{\partial \log \mathcal{Z}_A}{\partial \beta_A} = E. \quad (7)$$

Since the solution to the constrained optimization problem must be an exponential family, much like Boltzmann's distribution, the  $\varepsilon_j$  then play the role of the energy spectrum for a specific set of measurements. What is, then, the physical interpretation of  $\varepsilon_j$ ? And, can we

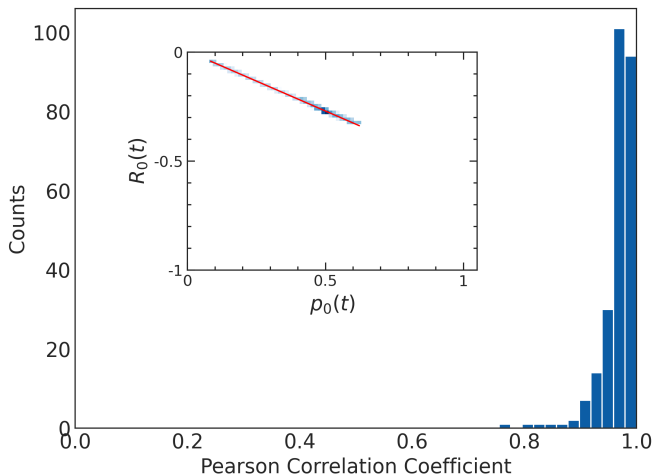


Figure 2: Here we provide support for the existence of a linear relationship between  $R_j$  and  $p_j$ . The main plot shows the histogram of the (absolute value of the) Pearson correlation coefficient of the sets  $\{p_j(t), R_j(t)\}$  for every (independent) eigenvalue of all observables considered, for all Hamiltonian models and initial states. Note that sets essentially corresponding to points or constant lines (i.e., cases where either standard deviation  $\Delta p_j$  or  $\Delta R_j$  is very small) have been excluded, as their Pearson coefficient would incorrectly indicate non-linearity. In the inset, we give as an example the 2D histogram of the time-implicit plot of  $(p_0(t), R_0(t))$  of the observable  $\sigma_0^y$  for model  $J = (0, 0, 1)$  &  $B = (0.9045, 0, 0.8090)$  and initial state corresponding to  $m = 10$ . Note we are using a logarithmic color scale, and the red line is a linear fit. We rescaled the extensive quantity  $R_j(t) \rightarrow R_j(t)/N$  to be able to compare it among different system sizes. In both plots, the system size is  $N = 20$ .

compute it without knowledge of the energy eigenstates? We now provide concrete answers to both questions.

First, we write explicitly  $\varepsilon_j$ :

$$\varepsilon_j = \frac{R_j^{DE}}{p_j^{DE}} = \sum_n \frac{|c_n|^2 [A_j]_{nn} E_n}{\sum_m |c_m|^2 [A_j]_{mm}} \quad (8)$$

Now, the equilibrium state  $\rho_{DE}$ , is identical to the post-measurement state obtained when we measure energy:  $\rho_{DE}$  is the diagonal part of  $|\psi_t\rangle\langle\psi_t|$ . We then build the equilibrium joint probability distribution of the energy eigenvalue and the  $j$ -th measurement outcome, by specifying the order of measurements as “energy first” and motivated by the fact that we are describing equilibrium:  $p_{eq}(E_n, j) := |c_n|^2 [A_j]_{nn}$ . Then, using Bayes’ theorem, we have

$$p_{eq}(E_n|j) := \frac{p_{eq}(E_n, j)}{\sum_n p_{eq}(E_n, j)} = \frac{|c_n|^2 [A_j]_{nn}}{\sum_m |c_m|^2 [A_j]_{mm}}. \quad (9)$$

The expectation value of the energy with the conditional distribution  $p_{eq}(E_n|j)$  is then  $\varepsilon_j$ :

$$\sum_n p_{eq}(E_n|j) E_n = \varepsilon_j \quad (10)$$

Hence,  $\varepsilon_j$  is the conditional expectation of the energy at fixed measurement outcome  $j$ . Or, equivalently,  $\varepsilon_j$  is the fraction of average energy stored, at equilibrium, in the eigenspace  $\mathcal{H}_j$ . Eventually, this leads to a neat interpretation of  $p_j^{DE}$ : it is a Boltzmann’s distribution of the measurement outcomes’ conditional energies  $\varepsilon_j$ . This is our second result. Uncovering  $\varepsilon_j$  as a novel notion of energy for  $A$ , at equilibrium, paints a compelling picture for the emergence of statistical mechanics (and thermodynamics) of observables, rather than states.

## 6. Computing $\varepsilon_j$

While understanding  $\varepsilon_j$  completes the theory at the conceptual level, having a way to compute it is paramount to leverage its predictive power. Here we provide a practical recipe based on the following analytical argument. First,  $\varepsilon_j$  must be approximately linear in the average energy:  $\varepsilon_j = \gamma_j E + \chi_j$ , at fixed  $p_j^{DE}$ . This can be seen from the constraint equation (7), or from eq.(6). However, at the most fundamental level, these equations are actually implicit and non-linear in  $\varepsilon_j$ , so  $\varepsilon_j$  can actually vary due to fluctuations. Nevertheless, for thermodynamically stable initial states (see Reimann’s work [1] and the discussion in section IC), we can see that  $\varepsilon_j$  can take values within the microcanonical window,  $\varepsilon_j \in [E - \Delta E/2, E + \Delta E/2]$ , with small fluctuations allowed. We then land on the empirically linear form

$$\varepsilon_j = \gamma_j E + \eta_j \Delta E + \chi_j. \quad (11)$$

It is important to highlight that the contribution from  $\Delta E$  is expected to be negligible in most cases. This is especially true in the macroscopic limit  $N \rightarrow \infty$ , where  $\Delta E/E \rightarrow 0$ . However, in some cases it must be taken into account, including when comparing situations in which we have the same average energy, but different fluctuations. In those cases,  $\eta_j$  will play a more important role in correctly estimating  $\varepsilon_j$ . Thus,  $\varepsilon_j$ ’s value is entirely determined by *at most* three coefficients  $\gamma_j, \eta_j, \chi_j$ , and very often  $\gamma_j$  and  $\chi_j$  are sufficient. For example, since we are exploring isolated quantum systems with initial states  $|\psi_0(\theta)\rangle$  numerical knowledge of two or three values of  $\varepsilon_j$  is sufficient to determine  $\varepsilon_j$  for all initial states. This can be seen in fig.3, where  $\varepsilon_j$  computed numerically is compared with its prediction from the analytical method described above: the predictions match the data extremely well. The inset shows  $\varepsilon_j^A(\theta_m)$  and  $E(\theta_m)$  plotted against the initial state in one case. The fits, found using eq.(11) and exact analytical expressions for  $E(\theta_m)$  and  $\Delta E(\theta_m)$  (given in appendix C), are clearly excellent. Additional data in support of these statements are shown in appendix A.

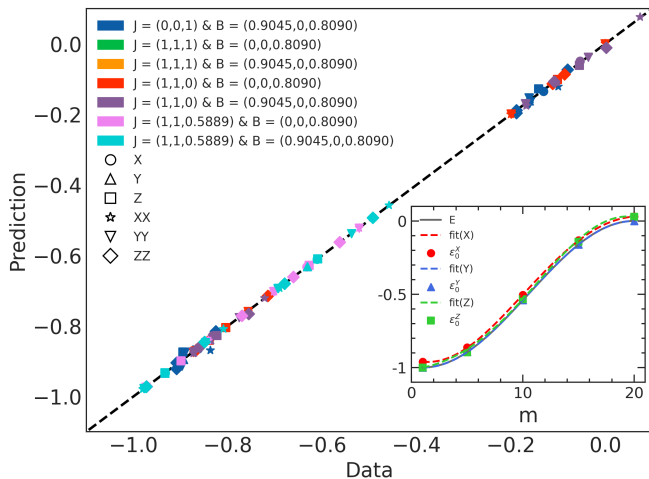


Figure 3: Implicit plot of our prediction for  $\varepsilon_j^A(\theta_m)$  given the fit obtained using eq.(11) against the numerical data, for  $N = 20$ . The plot includes  $\varepsilon_j$ 's for all (independent) eigenvalues of all observables, for all models and initial states. The black dashed line has been added for visual aid and represents a perfect prediction. We only include comparisons with the  $\varepsilon_j^{data}$  that were *not* used to determine the coefficients  $\gamma_j, \eta_j, \chi_j$ . In the inset, we show as an example a plot of  $\varepsilon_j^A(\theta_m)$  and  $E(\theta_m)$  against the initial state, parametrized by  $m$  (as described in subsection IIID), for the eigenvalue  $j = 0$  of one-body observables, model  $J = (0, 0, 1) \& B = (0.9045, 0, 0.8090)$  and  $N = 20$ . To make the plot more readable, we use the simplified notation  $X \equiv \sigma_0^x, Y \equiv \sigma_0^y$ , and  $Z \equiv \sigma_0^z$ . The coloured dashed lines are the fits to the data points given the function eq.(11). Note that we are using analytical expressions for the energy average  $E(\theta_m)$  and standard deviation  $\Delta E(\theta_m)$ , shown in appendix C. Note also that we divided by  $N$  the extensive quantities  $\varepsilon_j, E, \Delta E$  to be able to compare them among different system sizes.

### 7. Predictive power

We now test the predictive power of Observable Statistical Mechanics by putting the theoretical framework that has been laid out so far into work. For all observables, initial states, and Hamiltonian models, we first compute analytically  $\varepsilon_j$  using the method highlighted above, i.e., we obtain 3 data points  $\varepsilon_j^{data}$  from the numerics, and then we use them to compute the remaining  $\varepsilon_j$  using eq.(11). Once the  $\varepsilon_j$  are fixed, we find the Lagrange multiplier  $\beta_A$  that solves the energy constraint  $\sum_j p_j^{DE} \varepsilon_j = E$ . Then, we compare it with the time-average  $\overline{p_j(t)} := \frac{1}{T} \int_0^T p_j(t) dt$  obtained for sufficiently large values of  $T$  from the numerics. The comparison is made using the total variation distance between two probability distributions [91], i.e.,  $D(p, q) := \frac{1}{2} \sum_j |p_j - q_j|$ , and the results are summarized in figure 4. We observe a remarkable agreement with the theory, with  $D(p_j(t), p_j^{DE}) \leq 10^{-9}$  for all one-body observables, models and initial states considered. For two-body observables, the distance  $D(p_j(t), p_j^{DE})$  is generally higher

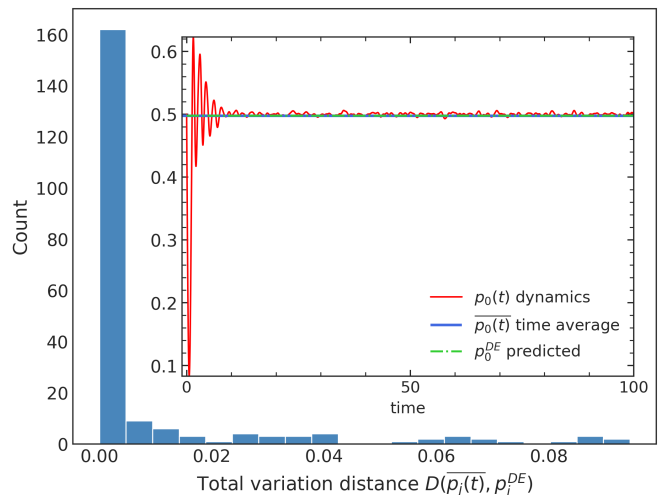


Figure 4: Histogram of the total variation distance  $D(p_j(t), p_j^{DE})$  for all observables, models and initial states considered, for  $N = 20$ . The inset shows as an example the time evolution of the exact probability distribution  $p_0(t)$ , together with its time average and our equilibrium prediction, for the observable  $\sigma_0^y$ , model  $J = (0, 0, 1) \& B = (0.9045, 0, 0.8090)$ , initial state  $m = 10$  and  $N = 20$ . Note that the x-axis has been limited to small values of the total variation distance.

than for the one-body, but overall there is good agreement with the theory's predictions, with  $\sim 80\%$  of values under  $10^{-2}$ . The data is shown as a histogram in the main plot of fig.4, which includes both one and two-body observables. The inset instead gives an example of the time evolution of the exact probability distribution  $p_j(t)$ . We see that after a short transient the probability exhibits small fluctuations around its equilibrium value, which agrees extremely well with the predictions of Observable Statistical Mechanics.

## II. DISCUSSION

We established Observable Statistical Mechanics: a new way to predict the equilibrium behavior of interacting, many-body, isolated quantum systems that do not require knowledge of the energy eigenstates. This is based on MOEP: an information-theoretic principle stating that the equilibrium measurement statistics are well-described by the distribution maximizing its entropy. The predictions of Observable Statistical Mechanics have been compared with numerical experiments, showing a remarkable capability to predict the equilibrium behavior of one-body and two-body observables in 7 different spin-1/2 Hamiltonian models and with 5 different initial states. At this point, a few comments are in order. First, we notice that the predictive power exhibited by Observable Statistical Mechanics is independent of system size. Indeed, this can be seen in fig.5, where we show our predictions hold for system sizes ranging from  $N = 10$  to

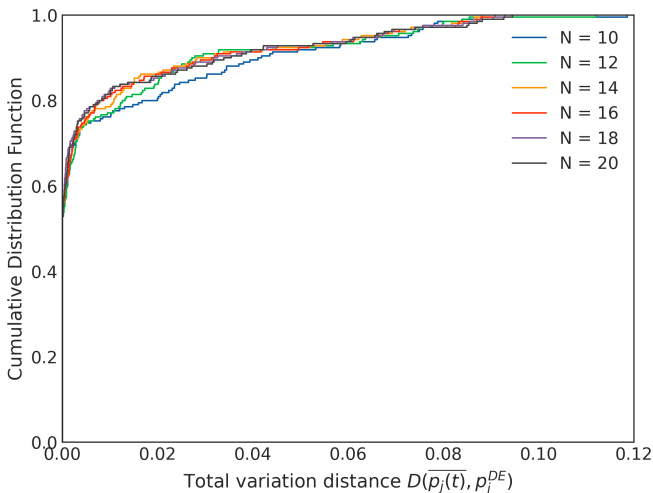


Figure 5: Comparison of the goodness of our prediction among system sizes ranging from  $N = 10$  to  $N = 20$ . The figure shows the cumulative distribution function of the total variation distance. We see we have similarly good agreement for all system sizes, slightly improving with increasing  $N$ . Note that the x-axis has been limited to small values of the total variation distance.

$N = 20$ . This is a great practical advantage since the exponential growth of the Hilbert space dimension is often the true bottleneck.

Second, the reason for the emergence of a maximum observable entropy principle in isolated many-body quantum dynamics is understood: it is due to the large degeneracy of realistic observables. This is absent in ordinary quantum statistical mechanics and is an element of novelty with respect to the standard characterization of quantum integrable vs. quantum chaotic systems, which is often used to discuss the nature of equilibrium. Observable Statistical Mechanics considers the dominant role played by measurements and aims at providing an accurate estimate of the stationary equilibrium distribution of a set of measurements, irrespective of the integrable or chaotic nature of the system.

Third, by changing the focus from states to measurement statistics, this work opens up new research avenues into foundational issues like equilibration, thermalization, and the nature of equilibrium. We now mention a few of them. Firstly, the observable-specific notion of energy that we introduced, the  $\varepsilon_j$ , is a novel quantity that deserves further study, including in other models. Given the crucial role it plays in predicting the equilibrium distribution, the empirical method provided to calculate it should be better understood, and it would be beneficial to find a fully analytical way of computing this quantity. Secondly, this new notion of energy suggests the possibility of a quantum thermodynamics based on on measurement statistics rather than density matrices. Indeed, we can define an observable free energy  $F_A$  via  $\mathcal{Z}_A := e^{-\beta_A F_A}$ . Then, summing both sides of eq.(3) over

$j$ , we find that at equilibrium we have

$$F_A = E - T_A \tilde{S}_A, \quad (12)$$

with the observable temperature  $T_A := \beta_A^{-1}$ . The emergence of this equilibrium relation, which is essentially a form of energy conservation, is a highly non-trivial result of Observable Statistical Mechanics. However, in order to have a complete picture we would need a kinetic, or operational, interpretation of the observable-specific thermodynamic quantities  $T_A$  and  $F_A$ . This is currently being developed and will be reported in future work. Finally, there has been significant interest lately on the effect of non-commuting charges (non-Abelian symmetries) on equilibration and thermalization [58, 92–97]. It would be interesting to explore the predictive power of Observable Statistical Mechanics in this case, and whether the presence of these more complex symmetries significantly affects the premises of the theory.

### III. METHODS

#### A. Validity of the Maximum Entropy Principle

In subsection IC we gave two heuristic arguments to support the use of the Maximum Observable Entropy Principle: one concerning the equilibrium mutual information between the observable and energy distributions, the other involving an entropic uncertainty principle. We now give the full version of these arguments.

##### 1. Defining joint, conditional and marginal probabilities

The study of equilibrium concerns the property of the Diagonal Ensemble  $\rho_{DE} := \sum_n |c_n|^2 |E_n\rangle\langle E_n|$ . This is the diagonal part of the time-dependent pure state  $|\psi_t\rangle$  in the energy basis and also the post-measurement state if we were to measure the energy of the system. Using the measurement interpretation we can compute the joint distribution of the energy and our observable by assuming the order “energy first”. This is because we are interested in equilibrium properties. Hence, we have that the energy marginal distribution is  $p_{eq}(E_n) = |c_n|^2$ , and the conditional is  $p_{eq}(j, s|E_n) = |\langle E_n|j, s\rangle|^2$ . Eventually, this leads to the following joint probability distribution at equilibrium:  $p_{eq}(E_n; j, s) = |c_n|^2 |\langle E_n|j, s\rangle|^2$ . From this we obtain the marginal  $p_{eq}(j, s)$  by summing over the energy variable:  $p_{eq}(j, s) = \sum_n |c_n|^2 |\langle E_n|j, s\rangle|^2$ .

The conditional probability of observing the  $n$ -th eigenvalues at equilibrium, given  $(j, s)$  can be computed by means of Bayes’ theorem:

$$p_{eq}(E_n|j, s) = \frac{p_{eq}(E_n; j, s)}{p_{eq}(j, s)} = \frac{|c_n|^2 |\langle E_n|j, s\rangle|^2}{\sum_m |c_m|^2 |\langle E_m|j, s\rangle|^2}. \quad (13)$$

Since the index  $s$  accounts for the degeneracy of the observables under study, it is also useful to compute the

equilibrium probability distributions that concern only the measurement outcomes. Hence, we have the additional probabilities  $p_{eq}(E_n; j) = |c_n|^2 [A_j]_{nn}$ ,  $p_{eq}(j) = \sum_n |c_n|^2 [A_j]_{nn}$ ,  $p_{eq}(E_n|j) = \frac{p_{eq}(E_n; j)}{p_{eq}(j)} = \frac{|c_n|^2 [A_j]_{nn}}{\sum_m |c_m|^2 [A_j]_{mm}}$ .

### 2. Zero Equilibrium Mutual Information for HUBs and HUOs

What's needed to make accurate predictions about equilibrium is in the energy eigenstates. However, our argument is that highly degenerate observables will be able to retain very little information about these. Certainly, not as many details as the energy eigenstates themselves. Therefore, instead of using all conserved quantities, knowledge of the average energy should be sufficient to make accurate predictions.

To support this line of thinking we compute two variants of the classical equilibrium mutual information between energy and observable. The first one  $\tilde{I}_{eq}(H, A)$  is about the mutual information between the energy and a full basis that diagonalizes our observables. The second one  $I_{eq}(H, A)$  is about the mutual information between the energy and the observable, disregarding the detailed information about the degeneracy.

We now compute these quantities for HUBs and HUOs, to check if the core intuition is correct. Recall a basis  $\{|j, s\rangle\}_{j=1, s=1}^{j=n_A, s=d_j}$  is a HUB if  $\langle E_n | j, s \rangle = \frac{e^{i\theta} j^s}{\sqrt{D}}$ , and an observable is HUO if it is diagonalized by a HUB [64]. This leads to  $p_{eq}(j, s) = p_{eq}(j, s|E_n) = \frac{1}{D}$ ,  $p_{eq}(E_n) = p_{eq}(E_n|j, s) = |c_n|^2$  and, similarly, for the coarse-grained distribution of outcomes of a HUO we find  $p_{eq}(j) = p_{eq}(j|E_n) = \frac{d_j}{D}$ ,  $p(E_n) = p_{eq}(E_n|j) = |c_n|^2$ .

Clearly, the measurement basis carries no information about the Hamiltonian basis, and viceversa: the conditionals are equal to the marginals. In other words, the two variables are independent. It's easy to see that the mutual information  $I(X, Y) := \sum p(X, Y) \log \left( \frac{p(X, Y)}{p(X)p(Y)} \right)$  is zero if and only if  $X$  and  $Y$  are independent random variables, so this implies

$$\tilde{I}_{eq}^{HUB}(H, A) = I_{eq}^{HUO}(H, A) = 0. \quad (14)$$

### 3. Equilibrium Mutual Information for Highly Degenerate Observables

We now generalize these arguments about the mutual information to general highly degenerate observables. To do so, we make use of the aforementioned Theorem 1 in [65], which says that for all subspaces such that  $d_j(d_j - 1) \geq D + 1$  there is a measurement basis such that  $|\langle E_n | j, s \rangle|^2 = \frac{[A_j]_{nn}}{d_j}$ . This leads to probability distributions that weigh equally all the different observable

degenerate states:

$$p_{eq}(E_n; j, s) = \frac{|c_n|^2 [A_j]_{nn}}{d_j} = \frac{p_{eq}(E_n, j)}{d_j} \quad (15)$$

$$p_{eq}(j, s) = \frac{\sum_n |c_n|^2 [A_j]_{nn}}{d_j} = \frac{p_{eq}(j)}{d_j} \quad (16)$$

$$p_{eq}(j, s|E_n) = \frac{[A_j]_{nn}}{d_j} = \frac{p_{eq}(j|E_n)}{d_j} \quad (17)$$

$$p_{eq}(E_n|j, s) = \frac{[A_j]_{nn} |c_n|^2}{\sum_m [A_j]_{mm} |c_m|^2} = p_{eq}(E_n|j) \quad (18)$$

This implies that  $\tilde{I}_{eq}(H, A) = I_{eq}(H, A)$ , as can be easily verified by direct calculation.

*Vanishing Mutual Information in the Thermodynamic Limit.* Note that the quantities  $\tilde{I}_{eq}(H, A)$  and  $I_{eq}(H, A)$  have very different scales. In fact, the mutual information is upper-bounded by the entropy marginals, namely  $\tilde{I} \leq \min\{\tilde{S}(A), S(H)\}$  and  $I \leq \min\{S(A), S(H)\}$ . However, while  $\tilde{S}(A) \leq \log D$  we have that  $S(A) \leq \log n_A \ll \log D$ . Nevertheless, since in this case these two mutual informations are equal, we just need to consider the scaling behaviour of  $S(A)$  and  $S(H)$ . The latter is expected to be extensive  $S(H) \sim N \sim \log D$ . However, realistic initial conditions have a relatively narrow energy distribution. This means  $S(H) \sim k_E N$  with  $k_E \ll 1$ . For the former, we note that in most experimental apparatus, our measurements will have at best  $n_A = N^k$  different outcomes, for some integer  $k \sim \mathcal{O}(1)$ . Thus,  $S(A) \leq \log n_A \sim \log N$ . The result of this reduced scaling compared to  $\tilde{S}(A)$ 's is that the mutual information vanishes in the thermodynamic limit:

$$\frac{\tilde{I}_{eq}(H, A)}{N} \leq \frac{\log n_A}{N} \xrightarrow{N \rightarrow \infty} 0 \quad (19)$$

Similarly, following Balz and Reimann [76], no realistic measurement can give us more than 20 relevant digits. Hence  $n_A < 10^{20}$ , which is independent of  $N$ . The conclusion is unchanged:  $\frac{\tilde{I}_{eq}(H, A)}{N} \xrightarrow{N \rightarrow \infty} 0$ .

As we approach the thermodynamic limit, in a macroscopically stable systems highly degenerate observables will not carry significant information about the distribution of energies. Therefore, when setting up our maximum entropy principle, the simple use of the average energy constraint should be sufficient.

*Finite-size argument.* The previous argument shows that, when considering larger and larger systems, we will eventually be justified to consider that our observables will be diagonalized by a basis that carries a negligible amount of information about the distribution of energies at equilibrium. However, this leaves open the question of what is the appropriate scale in which this becomes relevant. We now argue that the core argument can actually work rather well independent on the system size.



To see this, note that,

$$\tilde{I}_{eq} = I_{eq} = \sum_n |c_n|^2 [S(A) - S(A|E_n)], \quad (20)$$

with  $S(A|E_n) = -\sum_j p_{eq}(j|E_n) \log p_{eq}(j|E_n)$  the entropy of the distribution of the measurement outcomes conditioned on the  $n$ -th energy eigenspace. When  $|c_n|^2$  is a narrow energy distribution, concentrated around the mean value, and  $p_{eq}(A|E_n)$  does not fluctuate too much, then for all energy eigenvalues within a microcanonical window  $E_n \in [E - \Delta E/2, E + \Delta E/2]$  we will have  $p_{eq}(j|E_n) \approx \sum_m |c_m|^2 p_{eq}(j|E_m) = p_{eq}(j)$ , which leads to  $S(A) \approx \sum_n |c_n|^2 S(A|E_n)$  and eventually to  $I_{eq} \approx 0$ .

#### 4. Entropic Uncertainty Relation Argument

The previous argument regarding the equilibrium mutual information justifies our use of only two constraints in the entropy maximization problem for HUOs and, more generally, for highly degenerate observables. We shall now motivate the use of a maximum entropy principle for such observables in the first place, by showing  $\tilde{S}(A)$  is extensive in these cases. To do this, we use the entropic uncertainty relation  $\tilde{S}(A) + S(H) \geq -\log \tilde{c}(A, H)$ , where  $\tilde{c}(A, H) = \max_{j,s,n} |\langle j, s | E_n \rangle|^2$  [79, 80]. We can find an expression for  $\tilde{c}(A, H)$  for highly degenerate observables thanks to Theorem 1 in [65]. This states that when  $d_j(d_j - 1) \geq D + 1$  there is always a basis  $\{|j, s\rangle\}$  such that  $|\langle j, s | E_n \rangle|^2 = \frac{[A_j]_{nn}}{d_j}$ . This implies

$$-\log c(\tilde{A}, H) = -\log \left( \max_{j,n} \frac{[A_j]_{nn}}{d_j} \right) \quad (21)$$

$$\geq \min_j \log d_j - \log \max_{j,n} [A_j]_{nn}, \quad (22)$$

where we have used  $-\log \max_j a_j/b_j \geq -\log \max_j a_j / \max_j b_j$ . To evaluate the second term, we recall that  $[A_j]_{nn}$  is the distribution of measurement outcomes from a single energy eigenstate. Then, we find that  $-\log \max_{j,n} [A_j]_{nn} = -\min_n \log \max_j [A_j]_{nn} = \min_n S_\infty([A_j]_{nn})$ , where we have used the definition of min-entropy  $S_\infty([A_j]_{nn}) := -\log \max_j [A_j]_{nn}$  [98]. Thus, we have the following rigorous bound on  $\tilde{S}(A)$ :

$$\tilde{S}(A) \geq \max_j \log d_j + \min_n S_\infty([A_j]_{nn}) - S(H) \quad (23)$$

Let us look at each of the three terms on the right hand side individually.

- i) Looking at the first order in system size scaling, and remembering that we are addressing highly degenerate observables for which  $d_j(d_j - 1) \geq D - 1$ , in the regime  $d_j \gg 1$  we have  $d_j \sim D^{\kappa_j} \Rightarrow \log d_j \sim \kappa_j N$  with  $\frac{1}{2} \leq \kappa_j \leq 1$ .
- ii) Thanks to the Schur-concavity of the Rényi entropies, we know that minimum and maximum

value of  $S_\infty$  are achieved by the uniform distribution and by the Kronecker-delta distribution respectively, so  $S_\infty([A_j]_{nn}) \in [0, \log n_A]$ . Thus, as discussed for the Shannon entropy  $S(A)$  in III A 3, this term would give us at most a contribution of  $\mathcal{O}(\log N)$  for realistic measurements.

- iii) As mentioned in III A 3, under realistic conditions we expect  $S(H) \sim k_E N$  with  $k_E \ll 1$ .

Eventually, putting it all together, the dominant contribution for large  $N$  is

$$\tilde{S}(A) \geq \left( \max_j \kappa_j - k_E \right) N = \gamma N, \quad \gamma \in \mathcal{O}(1). \quad (24)$$

This argument agrees well with the scaling we obtain from the relation

$$\tilde{S}(A) = S(A) + \sum_j p_{eq}(j) \log d_j, \quad (25)$$

which can be found by applying the aforementioned Theorem 1 in [65] to the definition of  $\tilde{S}(A)$  at equilibrium. As stated previously,  $S(A) \in [0, \log n_A]$  will scale at most logarithmically in the system size  $\sim \log N$ , while the second term will scale like  $\sim \left( \sum_j p_j \kappa_j \right) N$ , with the sum being of  $\mathcal{O}(1)$  for an equilibrium probability distribution. An extensive entropy is the hallmark of statistical mechanics. This argument provides a rigorous basis to the intuition that, due to high degeneracy, equilibrium measurement statistics will have a highly entropic diagonalizing basis. In turn, this justifies the idea that accurate predictions at equilibrium can be made using the Maximum Observable Entropy Principle.

#### B. Derivation of the Equilibrium Equations

The original Equilibrium Equations were derived in [64] by maximizing  $S(A)$  under the constraints of state normalization and fixed average energy. Here we sketch the derivation of the Equilibrium Equations obtained by maximizing  $\tilde{S}(A)$  under the same constraints. The derivation is analogous to that in [64], so we refer the reader to that paper for the details.

We consider a generic mixed state  $\rho(t) = \sum_k q_k |\psi_k(t)\rangle \langle \psi_k(t)|$  and the entropy  $\tilde{S}(A)$ . Moreover, we define the quantity  $D_{js}^k := \langle j, s | \psi_k \rangle$  and its complex conjugate  $\overline{D_{js}^k}$ . The two constraints are

$$\mathcal{C}_N := \text{Tr}(\rho) - 1 \stackrel{!}{=} 0 \quad (26)$$

$$\mathcal{C}_E := \text{Tr}(\rho H) - E \stackrel{!}{=} 0. \quad (27)$$

We can then define the auxiliary function  $\Lambda_A[\rho; \lambda_N, \beta_A] := \tilde{S}(A) + \lambda_N \mathcal{C}_N + \beta_A \mathcal{C}_E$ , where  $\lambda_N$  and  $\beta_A$  are respectively, the Lagrange multipliers for the normalization and average energy constraint. Taking

derivatives of this function with respect to  $D_{js}^k$  and  $\overline{D_{js}^k}$ , and performing some algebraic manipulations, gives us

$$\text{Tr}(\rho[A_{js}, H]) \stackrel{\text{eq}}{=} 0 \quad (28)$$

$$-p_{js} \log p_{js} \stackrel{\text{eq}}{=} \lambda_A p_{js} + \beta_A R_{js} \quad (29)$$

where  $\lambda_A := (1 + \lambda_N)$ ,  $A_{js} := |j, s\rangle\langle j, s|$  and

$$R_{js} := \text{Tr}(\rho\{A_{js}, H\}) = \text{Cov}(A_{js}, H) + p_{js}E \quad (30)$$

with the anticommutator  $\{X, Y\} := \frac{XY+YX}{2}$  and the symmetrized covariance  $\text{Cov}(X, Y) := \langle\{X, Y\}\rangle - \langle X\rangle\langle Y\rangle$ . We note that the object  $R_{js}$  is an inner product between the operators  $A_{js}$  and  $H$  [99].

The first Equilibrium Equation, eq.(28), is about dynamical equilibration, i.e., it states that the distribution must be invariant under the unitary dynamics generated by  $H$ . Indeed, using von Neumann's equation one has  $i\hbar \frac{\partial}{\partial t} p_{js} \stackrel{\text{eq}}{=} 0$ . The second Equilibrium Equation characterizes the shape of  $p_{js}^{\text{eq}}$ . For example, if we sum over  $j, s$  we can see that the entropy of the equilibrium distribution has a thermodynamic flavor in the sense that it has a linear relation with the average energy:

$$\tilde{S}(A) \stackrel{\text{eq}}{=} \log \mathcal{Z}_A + \beta_A E, \quad (31)$$

where  $\beta_A$  plays the role of a measurement-specific inverse temperature and, calling  $\log \mathcal{Z}_A := \lambda_A$ ,  $\mathcal{Z}_A$  is a measurement-specific partition function.

From eq.(29), we can obtain eq.(3) by using Theorem 1 in [65], which implies  $p_{js}^{DE} = \frac{p_j^{DE}}{d_j}$  and  $R_{js}^{DE} = \frac{R_j^{DE}}{d_j}$ . This is equivalent to assigning to each degeneracy within the  $j$ -th eigenspace the same probability  $\frac{1}{d_j}$ , at equilibrium. This is related to the definition of the Observational Entropy [67–69, 100, 101]; see also eq.(25). And, indeed, this provides a physically meaningful mechanism for the emergence of this thermodynamic entropy — it corresponds to the Shannon entropy of the complete eigenbasis of an equilibrating and highly degenerate observable, computed on the diagonal ensemble

### C. Bound on $R_j$

Within a microcanonical energy window  $I_{mc} := [E - \frac{\Delta E}{2}, E + \frac{\Delta E}{2}]$ ,  $R_j \approx \sum_{E_n, E_m \in I_{mc}} c_n^* c_m e^{-i(E_m - E_n)t} \left(\frac{E_n + E_m}{2}\right) \langle E_n | A_j | E_m \rangle$  and  $\left(\frac{E_n + E_m}{2}\right) \in I_{mc}$  so we find the following straightforward bound

$$\left(1 - \frac{\Delta E}{2E}\right) p_j \lesssim \frac{R_j}{E} \lesssim \left(1 + \frac{\Delta E}{2E}\right) p_j \quad (32)$$

This implies the existence of some  $\varepsilon_j(t) \in I_{mc}$  such that  $R_j(t) \approx \varepsilon_j(t) p_j(t)$ . In the thermodynamic limit, for thermodynamically stable states, we also expect  $\Delta E/E \ll 1$ .

So we expect the bound to be more and more stringent as we increase the size of our system. This clearly shows that, assuming equilibration, we do expect eq.(6) to be satisfied. We therefore define the ratio  $\varepsilon_j(t) := R_j(t)/p_j(t)$  which, in general, exists (unless  $p_j(t) = 0$ ) and has the dimension of energy. While  $\varepsilon_j(t)$  exists, in principle it could fluctuate wildly, oscillate permanently, or exhibit other forms of dynamical behavior, rather than settling on a constant, as expected from eq.(6). Nevertheless, in section ID 4 we have provided strong numerical evidence to support the theoretical picture.

### D. Numerics

We now provide more details regarding the numerical simulations we have conducted. We have considered 7 one-dimensional spin-1/2 models described by Hamiltonians of the form

$$H = \sum_{i=0}^{N-1} \sum_{\alpha=x,y,z} (J^\alpha \sigma_i^\alpha \sigma_{i+1}^\alpha + B^\alpha \sigma_i^\alpha), \quad (33)$$

where  $i$  is an index that runs over the  $N$  lattice sites, and  $\sigma_i^\alpha$  ( $\alpha = x, y, z$ ) represents the Pauli operator with Pauli matrix  $\sigma^\alpha$  acting on the lattice site  $i$ , i.e.

$$\sigma_i^\alpha := \mathbb{I}^{\otimes i} \otimes \sigma^\alpha \otimes \mathbb{I}^{\otimes (N-1-i)}. \quad (34)$$

We use periodic boundary conditions, so that  $\sigma_N^\alpha = \sigma_0^\alpha$ . We denote the 7 models considered by their interaction coefficients  $J = (J^x, J^y, J^z)$  and their magnetic field coefficients  $B = (B^x, B^y, B^z)$ , which are shown in table I.

Model	$(J^x, J^y, J^z)$	$(B^x, B^y, B^z)$	Integrable?
Ising + LT	(0, 0, 1)	(0.9045, 0, 0.8090)	No [102, 103]
XXX + L	(1, 1, 1)	(0, 0, 0.8090)	Yes [104]
XXX + LT	(1, 1, 1)	(0.9045, 0, 0.8090)	Yes [104]
XX + L	(1, 1, 0)	(0, 0, 0.8090)	Yes [104]
XX + LT	(1, 1, 0)	(0.9045, 0, 0.8090)	No [105]
XXZ + L	(1, 1, 0.5889)	(0, 0, 0.8090)	Yes [104]
XXZ + LT	(1, 1, 0.5889)	(0.9045, 0, 0.8090)	No [105]

Table I: The 7 Hamiltonian models considered in the numerical simulations, classified in terms of their interaction and magnetic field coefficients. Of the models chosen, 3 are non-integrable and 4 are integrable. “L” and “LT” respectively refer to the presence of only a longitudinal field, or both longitudinal and transverse fields.

These models range from strongly non-integrable, such as in the case  $J = (0, 0, 1)$  &  $B = (0.9045, 0, 0.8090)$ , which is guaranteed to have such behaviour by [102, 103], to fully integrable models such as in the case  $J = (1, 1, 0)$  &  $B = (0, 0, 0.8090)$ .

To obtain the state dynamics, we use Trotterization [91], but we are guaranteed the error scales only linearly with the system size due to the form of the Hamiltonian (see the discussion in appendix B). We evolve the system up

to time  $t_f = 100$  with a timestep  $dt = 10^{-3}$ , resulting in 100,000 time points.

We have considered (even) system sizes from  $N = 10$  up to  $N = 20$  spins, and a class of initial states given by

$$|\psi_0(\theta_m)\rangle = R_y(\theta_m)^{\otimes N} |01\dots 01\rangle, \quad (35)$$

where  $R_y(\theta) = \exp(-iY\theta/2)$  is the rotation operator along the  $y$  axis [91] and  $\theta_m = \frac{m-1}{19}\frac{\pi}{2}$ . These states interpolate between the antiferromagnetic state along the  $z$  direction ( $\theta_1 = 0$ ) and the one along the  $x$  direction ( $\theta_{20} = \frac{\pi}{2}$ ). Note that the extremes are states of zero Shannon entropy for observables such as  $\sigma_i^z$  and  $\sigma_i^x$  respectively, thus maximally out of equilibrium for these observables. Throughout this study, we consider one-body observables  $\sigma_i^\alpha$  of the form given in eq.(34), and two-body observables of the form

$$\sigma_i^\alpha \sigma_{i+1}^\alpha = \mathbb{I}^{\otimes i} \otimes \sigma^\alpha \otimes \sigma^\alpha \otimes \mathbb{I}^{\otimes (N-2-i)}. \quad (36)$$

Their coarse-grained eigen-projectors are respectively

$$A_j^{\alpha,i} = \frac{\mathbb{I} + (-)^j \sigma_i^\alpha}{2} \quad (37)$$

$$A_{jk}^{\alpha,i} = A_j^{\alpha,i} A_k^{\alpha,i+1} \quad (38)$$

with  $j, k \in \{0, 1\}$ . Note this means that for two-body observables we have four distinct eigenvalues, i.e.,  $\{00, 01, 10, 11\}$ . Throughout the paper, we present only plots for the lattice site  $i = 0$ , as there is no difference between sites due to the translation invariance of the models.

To predict the equilibrium distribution  $p_j \propto e^{-\beta_A \varepsilon_j}$ , we first need to compute  $\varepsilon_j$  and then  $\beta_A$ . For the former, we first extract 3 data points from the numerics, either via a linear fit on the data  $\{p_j(t), R_j(t)\}$  or by taking

the ratio of the means  $\overline{R_j(t)}$  and  $\overline{p_j(t)}$ . Then, we use eq.(11) to compute the remaining  $\varepsilon_j$  for all initial states. For the latter,  $\beta_A$ , for one-body (i.e., binary ( $j = 0, 1$ )) observables we have an exact analytical solution

$$\beta_A = \frac{1}{\delta\varepsilon} \operatorname{arctanh}\left(\frac{\bar{\varepsilon} - E}{\delta\varepsilon}\right) = \frac{1}{\varepsilon_1 - \varepsilon_0} \ln\left(\frac{\varepsilon_1 - E}{E - \varepsilon_0}\right), \quad (39)$$

where  $\bar{\varepsilon} := \frac{\varepsilon_1 + \varepsilon_0}{2}$  and  $\delta\varepsilon := \frac{\varepsilon_1 - \varepsilon_0}{2}$ . For two-body observables, instead, we find the value of  $\beta_A$  by numerically optimizing eq.(7) with respect to it.

Finally, all extensive quantities at equilibrium have been rescaled by  $1/N$  to ensure that we can compare them among different system sizes.

## ACKNOWLEDGMENTS

L.S. thanks the ‘‘Angelo Della Riccia’’ Foundation for their continued support, and is grateful to Luis Pedro Garca Pintos, Samuel Slezak and Zoe Holmes for helpful discussions. F.A. acknowledges support from the Templeton World Charity Foundation under grant TWCF0336. F.A. would like to thank J.P. Crutchfield and C. Jarzynski for discussions about the dynamical emergence of thermal equilibrium. V.V. thanks the Gordon and Betty Moore Foundation and the Templeton Foundation for supporting his research. The authors would like to acknowledge the use of the University of Oxford Advanced Research Computing (ARC) facility in carrying out this work [106], and they are grateful to Tristan Farrow for providing them with access to this computing cluster. Finally, the authors acknowledge the use of Qibo [107, 108] in the simulations.

- 
- [1] P. Reimann, Physical Review Letters **101**, 190403 (2008), publisher: American Physical Society.
- [2] N. Linden, S. Popescu, A. J. Short, and A. Winter, Physical Review E **79**, 061103 (2009), publisher: American Physical Society.
- [3] S. Goldstein, J. L. Lebowitz, R. Tumulka, and N. Zanghı, The European Physical Journal H **35**, 173 (2010).
- [4] N. Linden, S. Popescu, A. J. Short, and A. Winter, New Journal of Physics **12**, 055021 (2010).
- [5] A. J. Short, New Journal of Physics **13**, 053009 (2011).
- [6] P. Reimann and M. Kastner, New Journal of Physics **14**, 043020 (2012), publisher: IOP Publishing.
- [7] P. Reimann, Physica Scripta **86**, 058512 (2012), publisher: IOP Publishing.
- [8] V. I. Yukalov, Laser Physics Letters **8**, 485 (2011), publisher: IOP Publishing.
- [9] H. Wilming, T. R. De Oliveira, A. J. Short, and J. Eisert, in *Thermodynamics in the Quantum Regime*, Vol. 195, edited by F. Binder, L. A. Correa, C. Gogolin, J. Anders, and G. Adesso (Springer International Publishing, Cham, 2018) pp. 435–455, series Title: Fundamental Theories of Physics.
- [10] C. Gogolin, *Equilibration and thermalization in quantum systems*, Ph.D. thesis, Freie Universitat Berlin (2014), accepted: 2018-06-08T01:06:39Z.
- [11] C. Gogolin and J. Eisert, Reports on Progress in Physics **79**, 056001 (2016), publisher: IOP Publishing.
- [12] J. Eisert, M. Friesdorf, and C. Gogolin, Nature Physics **11**, 124 (2015), number: 2 Publisher: Nature Publishing Group.
- [13] L. P. Garca-Pintos, N. Linden, A. S. Malabarba, A. J. Short, and A. Winter, Physical Review X **7**, 031027 (2017), publisher: American Physical Society.
- [14] L. D’Alessio, Y. Kafri, A. Polkovnikov, and M. Rigol, Advances in Physics **65**, 239 (2016), publisher: Taylor & Francis eprint: <https://doi.org/10.1080/00018732.2016.1198134>.
- [15] L. F. Santos and E. J. Torres-Herrera, in *Thermodynamics in the Quantum Regime*, Vol. 195, edited by F. Binder, L. A. Correa, C. Gogolin, J. Anders, and G. Adesso (Springer International Publishing, Cham, 2018) pp. 457–479, series Title: Fundamental Theories of Physics.

- [16] F. Borgonovi, F. Izrailev, L. Santos, and V. Zelevinsky, *Physics Reports* **626**, 1 (2016).
- [17] M. Berry, *Physica Scripta* **40**, 335 (1989).
- [18] F. H. L. Essler and M. Fagotti, *Journal of Statistical Mechanics: Theory and Experiment* **2016**, 064002 (2016).
- [19] L. Vidmar and M. Rigol, *Journal of Statistical Mechanics: Theory and Experiment* **2016**, 064007 (2016).
- [20] A. Polkovnikov, K. Sengupta, A. Silva, and M. Vengalattore, *Reviews of Modern Physics* **83**, 863 (2011), publisher: American Physical Society.
- [21] B. Sutherland, *Beautiful Models: 70 Years of Exactly Solved Quantum Many-Body Problems* (WORLD SCIENTIFIC, 2004).
- [22] J.-S. Caux and J. Mossel, *Journal of Statistical Mechanics: Theory and Experiment* **2011**, P02023 (2011).
- [23] J. M. Deutsch, *Physical Review A* **43**, 2046 (1991), publisher: American Physical Society.
- [24] J. M. Deutsch, *Reports on Progress in Physics* **81**, 082001 (2018), publisher: IOP Publishing.
- [25] M. Srednicki, *Physical Review E* **50**, 888 (1994), publisher: American Physical Society.
- [26] M. Srednicki, *Journal of Physics A: Mathematical and General* **29**, L75 (1996).
- [27] M. Srednicki, *Journal of Physics A: Mathematical and General* **32**, 1163 (1999).
- [28] M. Rigol, V. Dunjko, and M. Olshanii, *Nature* **452**, 854 (2008), number: 7189 Publisher: Nature Publishing Group.
- [29] M. V. Berry, *Journal of Physics A: Mathematical and General* **10**, 2083 (1977).
- [30] A. Voros, *Annales de l'institut Henri Poincaré. Section A, Physique Théorique* **26**, 343 (1977).
- [31] A. Shnirelman, *Uspekhi Mat. Nauk* **29**, 181 (1974).
- [32] P. Reimann, *Physical Review E* **97**, 062129 (2018).
- [33] P. Reimann, *Physical Review Letters* **120**, 230601 (2018), publisher: American Physical Society.
- [34] B. N. Balz, J. Richter, J. Gemmer, R. Steinigeweg, and P. Reimann, in *Thermodynamics in the Quantum Regime*, Vol. 195, edited by F. Binder, L. A. Correa, C. Gogolin, J. Anders, and G. Adesso (Springer International Publishing, Cham, 2018) pp. 413–433, series Title: Fundamental Theories of Physics.
- [35] C. Bartsch and J. Gemmer, *Physical Review Letters* **102**, 110403 (2009), publisher: American Physical Society.
- [36] P. Reimann, *Nature Communications* **7**, 10821 (2016), number: 1 Publisher: Nature Publishing Group.
- [37] S. Goldstein, T. Hara, and H. Tasaki, *New Journal of Physics* **17**, 045002 (2015), publisher: IOP Publishing.
- [38] S. Goldstein, J. L. Lebowitz, C. Mastrodonato, R. Tumulka, and N. Zanghi, *Physical Review E* **81**, 011109 (2010), publisher: American Physical Society.
- [39] J. von Neumann, *The European Physical Journal H* **35**, 201 (2010).
- [40] A. S. L. Malabarba, L. P. García-Pintos, N. Linden, T. C. Farrelly, and A. J. Short, *Physical Review E* **90**, 012121 (2014), publisher: American Physical Society.
- [41] M. L. Mehta, *Random matrices*, 3rd ed., Pure and applied mathematics No. v. 142 (Elsevier/Academic Press, Amsterdam San Diego, CA, 2004).
- [42] T. Guhr, A. Müller-Groeling, and H. A. Weidenmüller, *Physics Reports* **299**, 189 (1998).
- [43] L. Masanes, A. J. Roncaglia, and A. Acín, *Physical Review E* **87**, 032137 (2013), publisher: American Physical Society.
- [44] I. M. Khaymovich, M. Haque, and P. A. McClarty, *Physical Review Letters* **122**, 070601 (2019), publisher: American Physical Society.
- [45] H. A. Weidenmüller, *Journal of Physics A: Mathematical and Theoretical* **57**, 165002 (2024), publisher: IOP Publishing.
- [46] J. Wang, M. H. Lamann, J. Richter, R. Steinigeweg, A. Dymarsky, and J. Gemmer, *Physical Review Letters* **128**, 180601 (2022), publisher: American Physical Society.
- [47] R. Nandkishore and D. A. Huse, *Annual Review of Condensed Matter Physics* **6**, 15 (2015), eprint: <https://doi.org/10.1146/annurev-conmatphys-031214-014726>.
- [48] D. A. Abanin and Z. Papić, *Annalen der Physik* **529**, 1700169 (2017).
- [49] F. Alet and N. Laflorencie, *Comptes Rendus Physique Quantum simulation / Simulation quantique*, **19**, 498 (2018).
- [50] T. Mori, T. N. Ikeda, E. Kaminishi, and M. Ueda, *Journal of Physics B: Atomic, Molecular and Optical Physics* **51**, 112001 (2018), publisher: IOP Publishing.
- [51] M. Marcuzzi, J. Marino, A. Gambassi, and A. Silva, *Physical Review Letters* **111**, 197203 (2013), publisher: American Physical Society.
- [52] M. Gring, M. Kuhnert, T. Langen, T. Kitagawa, B. Rauer, M. Schreitl, I. Mazets, D. A. Smith, E. Demler, and J. Schmiedmayer, *Science* **337**, 1318 (2012), publisher: American Association for the Advancement of Science.
- [53] M. Serbyn, D. A. Abanin, and Z. Papić, *Nature Physics* **17**, 675 (2021).
- [54] S. Moudgalya, B. A. Bernevig, and N. Regnault, *Reports on Progress in Physics* **85**, 086501 (2022), publisher: IOP Publishing.
- [55] S. Moudgalya and O. I. Motrunich, *Physical Review X* **12**, 011050 (2022), publisher: American Physical Society.
- [56] B. Buča, J. Tindall, and D. Jaksch, *Nature Communications* **10**, 1730 (2019).
- [57] M. Medenjak, B. Buča, and D. Jaksch, *Physical Review B* **102**, 041117 (2020).
- [58] S. Majidy, Noncommuting charges' effect on the thermalization of local observables (2024), version Number: 2.
- [59] M. P. Fisher, V. Khemani, A. Nahum, and S. Vijay, *Annual Review of Condensed Matter Physics* **14**, 335 (2023).
- [60] F. Fritzsche and T. Prosen, *Physical Review E* **103**, 062133 (2021), publisher: American Physical Society.
- [61] Y. Li, X. Chen, and M. P. A. Fisher, *Physical Review B* **98**, 205136 (2018), publisher: American Physical Society.
- [62] B. Skinner, J. Ruhman, and A. Nahum, *Physical Review X* **9**, 031009 (2019), publisher: American Physical Society.
- [63] J. M. Koh, S.-N. Sun, M. Motta, and A. J. Minnich, *Nature Physics* **19**, 1314 (2023), publisher: Nature Publishing Group.
- [64] F. Anzà and V. Vedral, *Scientific Reports* **7**, 44066 (2017), number: 1 Publisher: Nature Publishing Group.
- [65] F. Anza, C. Gogolin, and M. Huber, *Physical Review Letters* **120**, 150603 (2018), publisher: American Physical Society.
- [66] F. Anza, *Pure states statistical mechanics: on its foundations and applications to quantum gravity*, <http://purl.org/dc/dcmitype/Text>, University of Oxford (2018).
- [67] D. Šafránek, J. M. Deutsch, and A. Aguirre, *Physical Review A* **99**, 012103 (2019), publisher: American Physical Society.

- Society.
- [68] P. Strasberg and A. Winter, PRX Quantum **2**, 030202 (2021), publisher: American Physical Society.
- [69] D. Šafránek, A. Aguirre, J. Schindler, and J. M. Deutsch, Foundations of Physics **51**, 101 (2021).
- [70] F. Meier, T. Rivlin, T. Debarba, J. Xuereb, M. Huber, and M. P. E. Lock, Emergence of a second law of thermodynamics in isolated quantum systems (2024), arXiv:2406.01677 [cond-mat, physics:quant-ph].
- [71] A. J. Short and T. C. Farrelly, New Journal of Physics **14**, 013063 (2012), publisher: IOP Publishing.
- [72] H. Tasaki, Physical Review Letters **80**, 1373 (1998), publisher: American Physical Society.
- [73] S. Goldstein, J. L. Lebowitz, R. Tumulka, and N. Zanghì, Journal of Statistical Physics **125**, 1193 (2006).
- [74] A. Peres, Physical Review Letters **49**, 1118 (1982), publisher: American Physical Society.
- [75] P. Reimann, New Journal of Physics **12**, 055027 (2010).
- [76] B. N. Balz and P. Reimann, Physical Review E **93**, 062107 (2016).
- [77] D. Hetterich, M. Fuchs, and B. Trauzettel, Physical Review B **92**, 155314 (2015), publisher: American Physical Society.
- [78] F. Anza, Entropy **20**, 744 (2018), number: 10 Publisher: Multidisciplinary Digital Publishing Institute.
- [79] S. Wehner and A. Winter, New Journal of Physics **12**, 025009 (2010).
- [80] P. J. Coles, M. Berta, M. Tomamichel, and S. Wehner, Reviews of Modern Physics **89**, 015002 (2017).
- [81] E. T. Jaynes, Physical Review **106**, 620 (1957), publisher: American Physical Society.
- [82] E. T. Jaynes, Physical Review **108**, 171 (1957), publisher: American Physical Society.
- [83] E. T. Jaynes, in *E. T. Jaynes: Papers on Probability, Statistics and Statistical Physics*, Synthese Library, edited by R. D. Rosenkrantz (Springer Netherlands, Dordrecht, 1989) pp. 39–76.
- [84] L. E. Reichl, *A Modern Course in Statistical Physics*, 1st ed. (Wiley, 2016).
- [85] T. M. Cover and J. A. Thomas, *Elements of Information Theory*, 1st ed. (Wiley, 2005).
- [86] I. Bengtsson, W. Bruzda, A. Ericsson, J.-A. Larsson, W. Tadej, and K. Życzkowski, Journal of Mathematical Physics **48**, 052106 (2007).
- [87] T. Durt, B.-G. Englert, I. Bengtsson, and K. Życzkowski, International Journal of Quantum Information **08**, 535 (2010), publisher: World Scientific Publishing Co.
- [88] Bandyopadhyay, Boykin, Roychowdhury, and Vatan, Algorithmica **34**, 512 (2002).
- [89] F. Anza, F. Pietracaprina, and J. Goold, Quantum **4**, 250 (2020), publisher: Verein zur Förderung des Open Access Publizierens in den Quantenwissenschaften.
- [90] M. G. Kendall, *The Advanced Theory of Statistics*, Vol. 1 (Griffin, 1948).
- [91] M. A. Nielsen and I. L. Chuang, *Quantum Computation and Quantum Information: 10th Anniversary Edition* (Cambridge University Press, 2010).
- [92] S. Majidy, W. F. Braasch, A. Lasek, T. Upadhyaya, A. Kalev, and N. Yunger Halpern, Nature Reviews Physics **5**, 689 (2023), number: 11 Publisher: Nature Publishing Group.
- [93] N. Yunger Halpern, M. E. Beverland, and A. Kalev, Physical Review E **101**, 042117 (2020), publisher: American Physical Society.
- [94] C. Murthy, A. Babakhani, F. Iniguez, M. Srednicki, and N. Yunger Halpern, Physical Review Letters **130**, 140402 (2023), publisher: American Physical Society.
- [95] I. V. Protopopov, W. W. Ho, and D. A. Abanin, Physical Review B **96**, 041122 (2017), publisher: American Physical Society.
- [96] J. D. Noh, Physical Review E **107**, 014130 (2023), publisher: American Physical Society.
- [97] F. Kranzl, A. Lasek, M. K. Joshi, A. Kalev, R. Blatt, C. F. Roos, and N. Yunger Halpern, PRX Quantum **4**, 020318 (2023), publisher: American Physical Society.
- [98] C. Arndt, *Information Measures* (Springer Berlin Heidelberg, Berlin, Heidelberg, 2001).
- [99] J. S. Sidhu and P. Kok, AVS Quantum Science **2**, 014701 (2020).
- [100] D. Šafránek, J. M. Deutsch, and A. Aguirre, Physical Review A **99**, 010101 (2019), publisher: American Physical Society.
- [101] J. Schindler, Basics of observational entropy (2020), arXiv:2010.00142 [quant-ph].
- [102] H. Kim and D. A. Huse, Physical Review Letters **111**, 127205 (2013), publisher: American Physical Society.
- [103] H. Kim, T. N. Ikeda, and D. A. Huse, Physical Review E **90**, 052105 (2014), publisher: American Physical Society.
- [104] F. Franchini, *An Introduction to Integrable Techniques for One-Dimensional Quantum Systems*, Lecture Notes in Physics, Vol. 940 (Springer International Publishing, Cham, 2017).
- [105] D. V. Dmitriev, V. Y. Krivnov, and A. A. Ovchinnikov, Physical Review B **65**, 172409 (2002).
- [106] A. Richards, University of Oxford Advanced Research Computing (2015).
- [107] S. Efthymiou, S. Ramos-Calderer, C. Bravo-Prieto, A. Pérez-Salinas, D. García-Martín, A. Garcia-Saez, J. I. Latorre, and S. Carrazza, Quantum Science and Technology **7**, 015018 (2022).
- [108] S. Efthymiou, M. Lazzarin, A. Pasquale, and S. Carrazza, Quantum **6**, 814 (2022).

## Appendix A: Additional numerical data

In this appendix, we provide additional numerical evidence supporting Observable Statistical Mechanics. We investigated 7 different Hamiltonian models, with system sizes from 10 to 20 (even only), initialized in 5 different initial states, and then studied the dynamics of the full probability distribution of 6 different observables. This amounts to 1260 long-time dynamics of probability distributions. Due to the large-scale nature of the numerical experiments, we cannot provide here figures for all data studied. Therefore, we only show selected additional figures to support and complement the plots shown in the main text. All data are available upon reasonable request to the authors.

### 1. Numerics

Before we show the additional data, here is a brief summary of the details of the numerics, for the reader's convenience. We have considered 7 one-dimensional spin-1/2 models described by Hamiltonians of the form

$$H = \sum_{i=0}^{N-1} \sum_{\alpha=x,y,z} (J^\alpha \sigma_i^\alpha \sigma_{i+1}^\alpha + B^\alpha \sigma_i^\alpha), \quad (\text{A1})$$

where  $i$  runs over the  $N$  lattice sites, and  $\sigma_i^\alpha$  ( $\alpha = x, y, z$ ) represents the Pauli operator with Pauli matrix  $\sigma^\alpha$  acting on the lattice site  $i$ , i.e.

$$\sigma_i^\alpha := \mathbb{I}^{\otimes i} \otimes \sigma^\alpha \otimes \mathbb{I}^{\otimes (N-1-i)}. \quad (\text{A2})$$

We use periodic boundary conditions, so that  $\sigma_N^\alpha = \sigma_0^\alpha$ . The 7 models considered have different interaction coefficients  $J = (J^x, J^y, J^z)$  and magnetic field coefficients  $B = (B^x, B^y, B^z)$ , which are shown in the following table.

Model	$(J^x, J^y, J^z)$	$(B^x, B^y, B^z)$	Integrable?
Ising + LT	(0, 0, 1)	(0.9045, 0, 0.8090)	No [1, 2]
XXX + L	(1, 1, 1)	(0, 0, 0.8090)	Yes [3]
XXX + LT	(1, 1, 1)	(0.9045, 0, 0.8090)	Yes [3]
XX + L	(1, 1, 0)	(0, 0, 0.8090)	Yes [3]
XX + LT	(1, 1, 0)	(0.9045, 0, 0.8090)	No [4]
XXZ + L	(1, 1, 0.5889)	(0, 0, 0.8090)	Yes [3]
XXZ + LT	(1, 1, 0.5889)	(0.9045, 0, 0.8090)	No [4]

Table II: The 7 Hamiltonian models considered in the numerical simulations, classified in terms of their interaction and magnetic field coefficients. Of the models chosen, 3 are non-integrable and 4 are integrable. ‘‘L’’ and ‘‘LT’’ respectively refer to the presence of only a longitudinal field or both longitudinal and transverse fields.

We evolve the system up to time  $t_f = 100$  with a timestep  $dt = 10^{-3}$ , resulting in 100,000 time points. We have considered (even) system sizes from  $N = 10$  up to  $N = 20$  spins, and a class of initial states given by

$$|\psi_0(\theta_m)\rangle = R_y(\theta_m)^{\otimes N} |01\dots 01\rangle, \quad (\text{A3})$$

where  $R_y(\theta) = \exp(-iY\theta/2)$  is the rotation operator along the  $y$  axis [5] and  $\theta_m = \frac{m-1}{19}\frac{\pi}{2}$ . These states interpolate between the antiferromagnetic state along the  $z$  direction ( $\theta_1 = 0$ ) and the one along the  $x$  direction ( $\theta_{20} = \frac{\pi}{2}$ ). Note that the extremes are states of zero Shannon entropy for observables such as  $\sigma_i^z$  and  $\sigma_i^x$  respectively, thus maximally out of equilibrium for these observables. We considered one-body observables  $\sigma_i^\alpha$  of the form given in eq.(A2), and two-body observables of the form

$$\sigma_i^\alpha \sigma_{i+1}^\alpha = \mathbb{I}^{\otimes i} \otimes \sigma^\alpha \otimes \sigma^\alpha \otimes \mathbb{I}^{\otimes (N-2-i)}. \quad (\text{A4})$$

### 2. Additional data

In fig.6 we give further evidence beyond what shown in the main text that indeed entropy is maximized, irrespective of the model considered. The same qualitative behavior can be seen for almost all other observables, models and initial states we investigated. Nevertheless, in fig.7 we show a rare case of the entropy not reaching equilibrium. It

is interesting to observe that this behavior emerges only for a specific combination of observables, models and initial states, and indeed the dependence on the initial state can clearly be seen in the figure. That is to say, having only knowledge of the model is insufficient to predict the equilibrium features of the entropy; one needs to specify the observable and the initial state too.

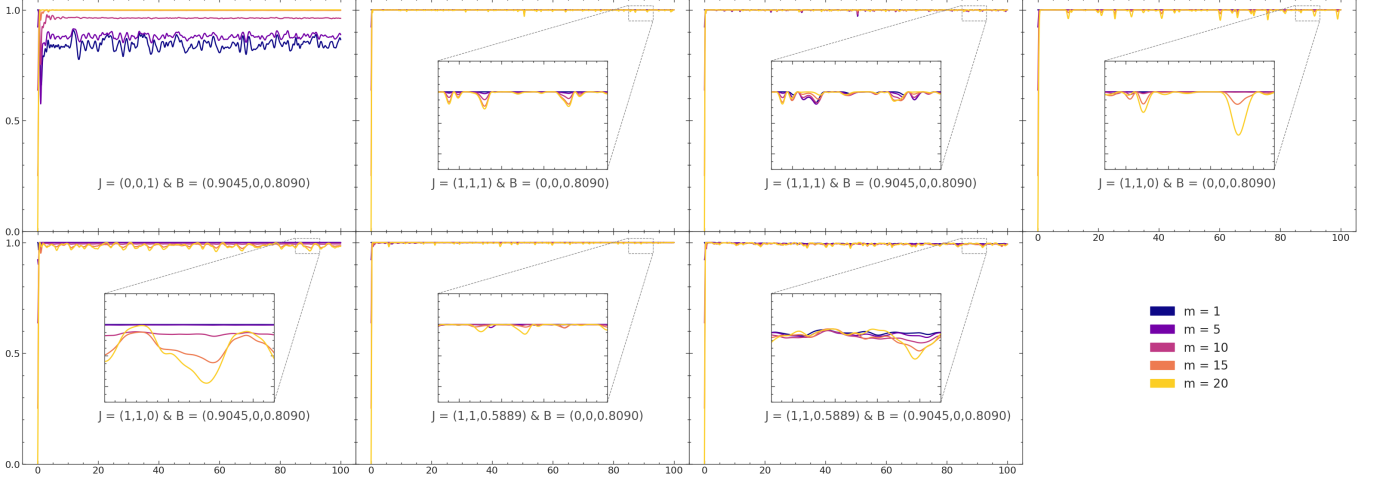


Figure 6: Here we show the time evolution of the Shannon entropy  $S(A)$  for the observable  $\sigma_0^x$  for all the models and initial states  $m$  considered, with  $N = 20$ . Each subplot corresponds to one of the Hamiltonians models we used. For the vast majority of other cases, we observe the same qualitative behavior, i.e., the entropy equilibrates around the maximum.

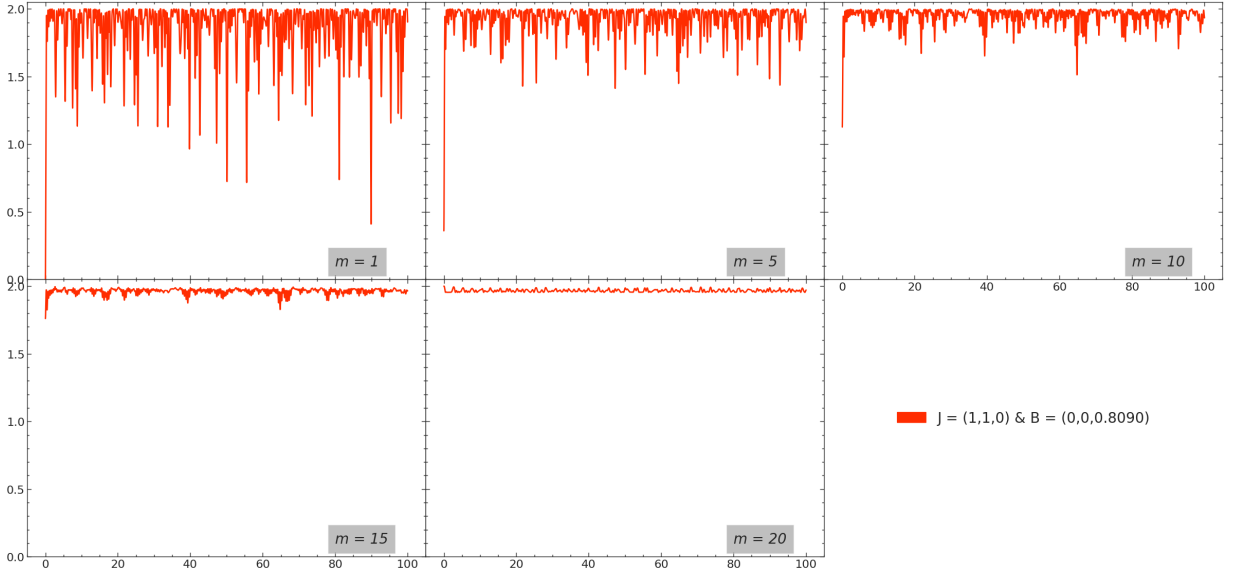
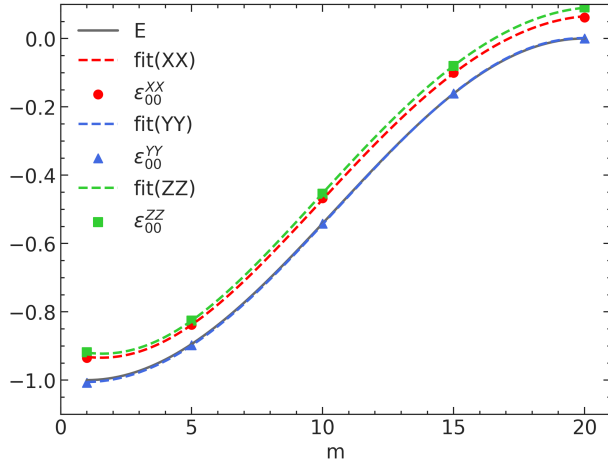
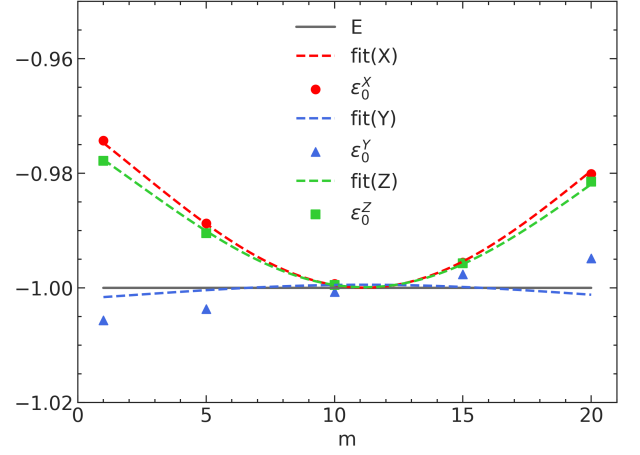


Figure 7: Here we give a rare example of the entropy  $S(A)$  not equilibrating. This plot corresponds to the observable  $\sigma_0^x \sigma_1^z$  for the model  $J = (1, 1, 0) \& B = (0, 0, 0.8090)$  and for all initial states  $m$  considered, with  $N = 20$ . Each subplot corresponds to one of the initial states we used. We note that whether the entropy equilibrates or not for this model depends on the initial state. The particular behavior we observe in this case might be due to the fact that this Hamiltonian is not only integrable, but can also be mapped to a non-interacting fermion model via a Jordan-Wigner transformation [3, 6].

Finally, to complement the plot of  $\varepsilon_j^A(\theta_m)$  and  $E(\theta_m)$  against  $m$  given in the main text, we here provide two additional examples. Fig.8a shows the plot for the same model previously considered, but this time for two-body observables. We note this is essentially the same behavior seen for one-body observables, and that this is true also for most other cases considered. On the other hand, the example shown in fig.8b corresponds to a model for which the energy is constant with respect to the initial state and therefore the dependence of  $\varepsilon_j$  on the energy standard deviation is more significant.



(a)  $\varepsilon_j^A(\theta_m)$  and  $E(\theta_m)$  against  $m$ , for the eigenvalue  $j = 00$  of two-body observables for the model  $J = (0, 0, 1)$  &  $B = (0.9045, 0, 0.8090)$ , with  $N = 20$ . To make the plot more readable, we use the simplified notation  $XX \equiv \sigma_0^x \sigma_1^x$ ,  $YY \equiv \sigma_0^y \sigma_1^y$ , and  $ZZ \equiv \sigma_0^z \sigma_1^z$ .



(b)  $\varepsilon_j^A(\theta_m)$  and  $E(\theta_m)$  against  $m$ , for the eigenvalue  $j = 0$  of one-body observables for the model  $J = (1, 1, 1)$  &  $B = (0.9045, 0, 0.8090)$ , with  $N = 20$ . We use the simplified notation  $X \equiv \sigma_0^x$ ,  $Y \equiv \sigma_0^y$ , and  $Z \equiv \sigma_0^z$ . Note the range of the  $y$  axis is very small.

Figure 8: We here give additional examples of plots of  $\varepsilon_j^A(\theta_m)$  and  $E(\theta_m)$  against the initial state, parametrized by  $m$  (as described in subsection A 1). In 8a, we show this plot for two-body observables for a specific model, whereas in 8b we pick a model in which the average energy is constant and thus the energy standard deviation plays a bigger role. The coloured dashed lines are the fits to the data points given the function  $\varepsilon_j = \gamma_j E + \eta_j \Delta E + \chi_j$ . Note that we are using analytical expressions for the energy average  $E(\theta_m)$  and standard deviation  $\Delta E(\theta_m)$ , shown in appendix C. Note also that we divided by  $N$  the extensive quantities  $\varepsilon_j, E, \Delta E$  to be able to compare them among different system sizes.

## Appendix B: Error scaling in Trotterization

Given a Hamiltonian that is expressed as a sum of local terms, we want to justify the use of Trotterization to simulate the time evolution. We are considering Hamiltonians of the form (A1) with periodic boundary conditions, which indeed can be expressed as sums of local terms, i.e.,

$$H = \sum_{i=0}^{N-1} h_i. \quad (\text{B1})$$

Using the tools developed in [7] we can analyze the error of Trotterization on this class of Hamiltonians. Specifically, we know that the error  $\epsilon$  scales as:

$$\epsilon = \mathcal{O}\left(\frac{\alpha t_f^2}{r}\right), \quad (\text{B2})$$

where  $t_f$  is the simulation time,  $r$  is the number of Trotter steps, and  $\alpha$  is a Hamiltonian specific factor. In order to understand the scaling of the error as a function of  $N$ , we need to explicitly calculate  $\alpha$ . The definition of  $\alpha$  is given as

$$\alpha := \sum_{p,q=1}^N \|[h_p, h_q]\|. \quad (\text{B3})$$

For the Hamiltonian we are concerned with,

$$\|[h_p, h_q]\| = \begin{cases} 0 & p = q \\ a & q = p \pm 1 \\ 0 & \text{otherwise} \end{cases} \quad (\text{B4})$$

where  $a$  is just some scalar that depends on  $J = (J_x, J_y, J_z)$  and  $B = (B_x, B_y, B_z)$  but crucially does not depend on  $N$ . We see that the only contributions to  $\alpha$  come from the commutator between terms in the Hamiltonian that have



overlapping support. A simple counting argument shows that for  $N$  sites, there are  $2N$  combinations of overlapping terms. Therefore,  $\alpha = 2aN$ . This means that the error can be written as

$$\epsilon = \mathcal{O}\left(\frac{2aN t_f^2}{r}\right) \quad (\text{B5})$$

We conclude that the Trotter error only grows linearly with the number of sites  $N$ .

### Appendix C: Analytical expressions for $E(\theta_m)$ and $\Delta E^2(\theta_m)$

Here we provide the analytical expressions we have obtained for the average energy  $E(\theta_m)$  and the energy variance  $\Delta E^2(\theta_m)$  in terms of their dependence on  $\theta_m$ , which parametrizes the class of initial states that we are considering; see eq.(A3).

For this family of initial states and for the class of Hamiltonians  $H$  defined in eq.(A1), we have that

$$\begin{aligned} E(\theta_m) &:= \text{Tr}(\rho_0(\theta_m)H) = \\ &= -J^x \sin^2(\theta_m) - J^z \cos^2(\theta_m) \\ &+ \frac{\llbracket N \text{ is odd} \rrbracket}{N} [B^x \sin(\theta_m) + B^z \cos(\theta_m)] \end{aligned} \quad (\text{C1})$$

and

$$\begin{aligned} \Delta E^2(\theta_m) &:= \text{Tr}(\rho_0(\theta_m)H^2) - E^2(\theta_m) = \\ &= \frac{1}{N} \sum_{\alpha=x,y,z} [(J^\alpha)^2 + (B^\alpha)^2] \\ &+ \frac{2}{N} [(J^x)^2 + J^z J^y] \sin^2(\theta_m) \\ &+ \frac{2}{N} [(J^z)^2 + J^x J^y] \cos^2(\theta_m) \\ &- \frac{3}{N} [J^x \sin^2(\theta_m) + J^z \cos^2(\theta_m)]^2 \\ &- \frac{1}{N} [B^x \sin(\theta_m) + B^z \cos(\theta_m)]^2 \\ &- \frac{2\llbracket N \text{ is odd} \rrbracket}{N^2} [J^x B^x \sin(\theta_m) + J^z B^z \cos(\theta_m)] \end{aligned} \quad (\text{C2})$$

where the Iverson bracket is defined as

$$\llbracket P \rrbracket := \begin{cases} 1 & \text{if } P \text{ is true} \\ 0 & \text{otherwise} \end{cases}$$

and  $N$  is the system size.

- 
- [1] H. Kim and D. A. Huse, Physical Review Letters **111**, 127205 (2013), publisher: American Physical Society.
  - [2] H. Kim, T. N. Ikeda, and D. A. Huse, Physical Review E **90**, 052105 (2014), publisher: American Physical Society.
  - [3] F. Franchini, *An Introduction to Integrable Techniques for One-Dimensional Quantum Systems*, Lecture Notes in Physics, Vol. 940 (Springer International Publishing, Cham, 2017).
  - [4] D. V. Dmitriev, V. Y. Krivnov, and A. A. Ovchinnikov, Physical Review B **65**, 172409 (2002).
  - [5] M. A. Nielsen and I. L. Chuang, *Quantum Computation and Quantum Information: 10th Anniversary Edition* (Cambridge University Press, 2010).
  - [6] P. Jordan and E. Wigner, Zeitschrift fur Physik **47**, 631 (1928).
  - [7] A. M. Childs, Y. Su, M. C. Tran, N. Wiebe, and S. Zhu, Physical Review X **11**, 011020 (2021), publisher: American Physical Society.